
DETECTION AND ESTIMATION OF SPACECRAFT MANEUVERS FOR CATALOG MAINTENANCE *

Laura Pirovano, Roberto Armellin

Te Pūnaha Ātea - Space Institute
The University of Auckland
Auckland, New Zealand

{ laura.pirovano, roberto.armellin}@auckland.ac.nz

ABSTRACT

Building and maintaining a catalog of resident space objects involves several tasks, ranging from observations to data analysis. Once acquired, the knowledge of a space object needs to be updated following a dedicated observing schedule. Dynamics mismodeling and unknown maneuvers can alter the catalog's accuracy, resulting in uncorrelated observations originating from the same object. Starting from two independent orbits, this work presents a novel approach to detect and estimate maneuvers of resident space objects, which allows for correlation recovery. The estimation is performed with successive convex optimization without a-priori assumption on the thrust arcs structure and thrust direction.

Keywords Maneuver detection · Maneuver estimation · data association · trajectory optimization · convex optimization.

List of Acronyms

AIDA Accurate Integrator for Debris Analysis

CC cartesian coordinates

CDM control distance metric

COE classical orbital elements

CUT Conjugate Unscented Transform

DA Differential Algebra

DALS Differential Algebra Least Squares

DMC dynamic model compensation

DoF degrees of freedom

DTA Defence Agency Technology

ECI Earth-centered inertial

EWSK east-west station-keeping

GEO geostationary Earth orbit

GTO geostationary transfer orbit

IOD initial orbit determination

LEO low Earth orbit

LP Linear Programming

LT low-thrust

MC Monte Carlo

MEE modified equinoctial elements

NLP Nonlinear Programming Problem

NP non-polynomial

OCP optimal control problem

OD orbit determination

SDP Semidefinite programming

SNC state noise compensation

SOCP Second-Order Cone Programming

SRP solar radiation pressure

STM state transition matrix

TLE Two-Line Element

TPBVP two-points boundary value problem

UCT Uncorrelated Track

VLT very low-thrust

*© 2022 IEEE. Personal use of this material is permitted. Permission from IEEE must be obtained for all other uses, in any current or future media, including reprinting/republishing this material for advertising or promotional purposes, creating new collective works, for resale or redistribution to servers or lists, or reuse of any copyrighted component of this work in other works.

1 Introduction

The space population is rapidly increasing. As of June 2022, more than 45.000 objects larger than 10 cm are being tracked in space², and the active space population has doubled in the last four years. With the current development and deployment of very large constellations, it is clear that the safety and stability of operations need to be improved to allow long-term sustainability of space activities. To do so, an accurate catalog of all resident space objects is fundamental, which requires initialization of newly discovered tracks [1–3], correlation between tracks [4], and linkage of new observations to known orbits [5]. Once initialized, the catalog needs to be maintained through careful scheduling for object tracking. However, operational spacecraft perform frequent maneuvers, usually dictated by mission requirements or collision avoidance, potentially creating double entries in the catalog with post-maneuver measurements and thus hindering the data association problem. Recovering data association with the assumption of unknown maneuvers is thus fundamental to keep the catalog up-to-date and will be the focus of this manuscript.

Past efforts in maneuver detection started from linked orbits to analyze the performance of satellites. Patera [6] found maneuvers by identifying anomalous deviations between the published values of an orbital parameter and the corresponding values given by polynomial fitting of the moving window curve fit technique. Lemmens and Krag [7] addressed maneuver detection for low Earth orbits (LEOs) detecting space events based on analyzing their Two-Line Elements (TLEs) history. However, the most challenging aspect of maneuver detection is understanding whether two Uncorrelated Tracks (UCTs) can be linked using a maneuver, thus regaining data association through the assumption of a maneuver, rather than detecting maneuvers between two orbits known to be the same object.

The most studied methods for dealing with uncertain dynamics in the state estimation process include the use of state noise compensation (SNC), that is the addition of white noise to the process, and dynamic model compensation (DMC), which yields a deterministic acceleration term as well as a purely random term [8]. However, they are not suitable for the problem at hand. Indeed, while effectively preventing divergence due to mismodeling, adding process noise does not provide a method for estimating the mismodeling or detecting its presence. On the other hand, DMC requires a significant amount of tuning, and appending dynamics parameters to the state requires a known model for those modeled dynamics [9].

Lately, optimal control distance metrics (CDMs) approaches [9–11] were shown to be suitable for detecting and characterizing maneuvers of UCTs in the absence of full orbit solutions. In [10] it is assumed that the object which realizes the measurement with the least energy consumption, in linearized dynamics is the most likely originator. Furthermore, it gives a way to determine the probability that the nominal cost (a possible maneuver) is greater than the system uncertainty, hence considering non-perfect data association, with Gaussian assumption. In this way, the approach can reconstruct maneuvers with no a-priori knowledge. In [9] Lubey extended the CDM approach to include several perturbations and adapted it to estimate unmodeled dynamics - not only maneuvers. However, Singh et al. in [11] showed that an energy-based metric rather than a propellant consumption-based one significantly deteriorates the quality of the reconstructed maneuvers. To avoid this issue, they formulated a Nonlinear Programming Problem (NLP) problem, a step that affects their approach's efficiency and robustness. In summary, CDMs approaches provide data-driven capabilities for detecting and characterizing unknown maneuvers. However, there is overall a lack of a methodology meeting all the following requirements:

- use ΔV as a metric to enable a more reliable indicator of track correlation and a more realistic maneuver estimation,
- avoid linearized and/or simplified dynamics to potentially handle large uncertainties and data sparsity,
- work for arbitrary statistics,
- is numerically efficient and robust to be used in routine operations.

This is the gap that this manuscript covers: following the definition of a reference trajectory with accurate dynamics, any deviation from it is propagated, and a minimum-fuel path is found through (successive) convex optimization. Focus is posed on the choice of coordinates for which a single iteration is enough to reach convergence. Within a single convexification, indeed, polynomial run time and global convergence are ensured. Two methods are then introduced to transfer the state uncertainty into maneuver uncertainty: the Mahalanobis distance approach and the Conjugate Unscented Transform (CUT), which respectively deal with the detection and the estimation parts.

The paper is organized as follows. Section 2 describes the mathematical model for the fuel-optimal maneuver pattern to fit two states at different epochs, where the optimal control problem (OCP) is transformed from a NLP to a

²Source: www.space-track.org

Second-Order Cone Programming (SOCP) one. Section 3 introduces the Mahalanobis distance and CUT approaches, defining the different constraints to follow the two methods. The full optimization algorithm is shown in Section 4. Results are shown in Section 5, where maneuvers are reconstructed for a synthetic maneuver, for a routine east-west station-keeping (EWSK) maneuver in geostationary Earth orbit (GEO) and for a low-thrust (LT) orbit raising of a highly-elliptical orbit. Lastly, conclusions are drawn in Section 6.

2 Dynamics of a maneuvering object

This section explains the dynamical models and approaches followed to build the optimization problem. Section 2.1 introduces the formulation of a nonlinear OCP, and defines the core constraints and objective of the maneuver detection problem. Section 2.2 discretizes the problem, which is then convexified in Section 2.3.

2.1 Formulation of the nonlinear OCP

The problem of finding maneuver patterns that connect two defined states (x_0, x_1) given the time of flight (Δt) is an OCP with boundary constraints. Being the two available states the result of two independent orbit determinations (ODs), neighboring values of the reference states can be explored within a set \mathcal{X} , hence introducing uncertain boundary constraints. Assuming operators implement optimal maneuvers, the following nonlinear OCP with boundary value conditions can be formulated, with the task of minimizing propellant use:

$$\min_u J(x, u, p \mid x_0, x_1, t_0, t_f) \quad (1a)$$

$$\text{s.t. } \dot{x}(t) = f(x, u, p, t), \quad (1b)$$

$$(x(t), u(t), t) \in \mathcal{C}^i(t), \quad \forall t \in \mathbb{R}_{\Delta t}, i \in \mathbb{N}_0 \quad (1c)$$

$$x_{t_0} \in \mathcal{X}_{t_0}, \quad x_{t_f} \in \mathcal{X}_{t_f}. \quad (1d)$$

The cost in Eq. (1a) describes the goal of the mission to minimize the use of propellant, given the boundary conditions in terms of state and time. Equation (1b) describes the system dynamics, which is composed of natural motion, spacecraft control u and any other parameters p . Equation (1c) ensures continuity or higher differentiability of the trajectory. Lastly, Eq. (1d) bounds the initial and final states' variation. Each equation of Problem 1 is now described.

Minimization function (Eq. (1a)) the typical minimization function of a minimum fuel OCP is

$$\Delta V = \int_{t_0}^{t_f} \|\mathbf{u}(\tau)\| d\tau, \quad (2)$$

that is the total thrusting ΔV over the arc $T = [t_0, t_f]$.

State dynamics (Eq. (1b)) It is fundamental that the natural motion of the body is accurately described, to avoid overloading the control with unmodeled known dynamics, resulting in a non-realistic ΔV profile. For this reason, the dynamics are described with the numerical propagator Accurate Integrator for Debris Analysis (AIDA) [12], which implements the following acceleration vector

$$\mathbf{a}_{\text{AIDA}} = \mathbf{a}_{\oplus} + \mathbf{a}_{\text{drag}} + \mathbf{a}_{\odot} + \mathbf{a}_{\text{☾}} + \mathbf{a}_{\text{SRP}} = \mathbf{f}(\mathbf{x}, t), \quad (3)$$

whose components are:

\mathbf{a}_{\oplus} Earth's gravity potential up to order 15,

\mathbf{a}_{drag} drag with NRLMSISE-00 atmospheric density model,

$\mathbf{a}_{\odot, \text{☾}}$ third-body perturbing accelerations - Sun and Moon - with NASA's SPICE³ toolkit [13],

\mathbf{a}_{SRP} solar radiation pressure (SRP) with dual-cone shadow model.

The acceleration is expressed in Earth-centered inertial (ECI) coordinates and the dynamics is integrated with a Runge-Kutta 7-8 scheme. The control is then added to the natural motion of the body.

³<https://naif.jpl.nasa.gov/naif/toolkit.html>

Boundary conditions (Eq. (1d)) The boundary conditions are the results of two independent ODs. Assuming they can be modeled as multivariate Gaussian random variables, they can be defined by their mean, $\boldsymbol{\mu}_{t_0}$ and $\boldsymbol{\mu}_{t_f}$, and covariance Σ_{t_0} and Σ_{t_f} , which are positive definite matrices. It is then possible to bound the variation from the mean values with a χ -square quantile of level α and 6 degrees of freedom (DoF):

$$\frac{1}{2}(\mathbf{x}_i - \boldsymbol{\mu}_{t_j})^T \Sigma_{t_j} (\mathbf{x}_i - \boldsymbol{\mu}_{t_j}) \leq q_{\chi^2}(\alpha, 6) = \mathcal{M}, \quad j = \{0, f\}, i = \{0, N\}. \quad (4)$$

Despite the problem being now fully defined, in most cases, the solution of such an optimal control problem requires time consuming numerical procedures [14]. This is because traditional methods to solve this type of problem - indirect and direct - either result in two-points boundary value problems (TPBVPs) highly sensitive to initial guesses, or are non-polynomial (NP) hard, which means that the amount of computation required to solve the problem will not be limited by a bound determinable a priori. Unknowable computational time and lack of assured algorithm convergence are the kinds of obstacles that would preclude its applications in aerospace engineering problems that demand reliable and rapid solutions [15]. Instead, the following sections will show how to solve Problem 1, by firstly discretizing the NLP problem and then transforming it into a (successive) convex one. For a single convex optimization problem convergence is guaranteed to a global minimum in polynomial time.

2.2 Discretizing the dynamics of the nonlinear OCP

In this section, Problem 1 will be transformed from infinite-dimensional to finite-dimensional by discretizing the trajectory into a finite number of nodes $N + 1$, assuming that the control can only assume a fixed value within each segment, between two consecutive nodes. The initial node \mathbf{x}_0 is then defined at the earliest epoch t_0 , while the last node \mathbf{x}_N at the second epoch t_f . The optimization variables are then $9(N + 1)$, being the state \mathbf{x}_k and the control \mathbf{u}_k at each node k , while the minimization function becomes the sum of the contributions of the control over the segments. Problem 1 then becomes:

$$\min \sum_{i=0}^N \|\mathbf{u}_i\| \cdot \Delta t \quad (5a)$$

$$\text{s.t. } \mathbf{f}_i = \mathbf{a}_{\oplus, i} + \mathbf{a}_{\text{drag}, i} + \mathbf{a}_{3B, i} + \mathbf{a}_{\text{SRP}, i} + \mathbf{u}_i \quad i \in \mathbb{N}_{[0, N]} \quad (5b)$$

$$\mathbf{x}_{i+1} = \mathbf{x}_i + \int_i^{i+1} \mathbf{f}_i(\mathbf{x}, \mathbf{u}_i, t) dt \quad i \in \mathbb{N}_{[0, N]-1} \quad (5c)$$

$$\frac{1}{2} \|F_{t_j}(\mathbf{x}_i - \boldsymbol{\mu}_{t_j})\| \leq \mathcal{M}, \quad F_{t_j} = \sqrt{\Sigma_{t_j}}, \quad j = \{0, f\}, i = \{0, N\}. \quad (5d)$$

2.3 Problem convexification

The discretized problem in Section 2.2 is still a NLP problem, with NP computational time and lack of assured algorithm convergence. However, by carefully choosing the type of constraints, coordinates and minimization function, it is possible to obtain a convex problem, for which the following properties hold:

- if a feasible solution exists, it is the global optimum;
- the run time complexity is polynomial;
- there is no need for an initial guess.

These properties ensure global convergence and efficiency, which is why many aerospace applications make use of it, from low-thrust trajectory optimization [16], to asteroid hopping transfers designs [17], soft landings [18] and autonomous collision avoidance [19], to name a few. It is to be noted that there are three types of convex optimization: Linear Programming (LP), SOCP, and Semidefinite programming (SDP), with the first one being the most optimized and the latter being the one with the most modeling power. In return, the first may be insufficient to model complex problems, while for the latter existing algorithms still do not scale well to the problem size, meaning the solution speed deteriorates rapidly as the problem size increases. For this reason, SOCPs are attractive because they hold a good balance between the other two types of convex optimization.

This section introduces the mathematical operations to turn Problem 5 into a SOCP problem:

$$\min \mathbf{c}^T \mathbf{x} \quad (6a)$$

$$\text{s.t. } A\mathbf{x} = \mathbf{b} \quad (6b)$$

$$\|F_i \mathbf{x} + \mathbf{d}_i\| \leq \mathbf{p}_i^T \mathbf{x} + q_i, \quad i \in \mathbb{N}_{[1: L]} \quad (6c)$$

where the objective function is linear and constraints are linear and second-order cones. Equation (6c) is called a rotated quadratic cone \mathcal{Q}_r^{n+1} , where n is the dimensionality of \mathbf{x} . Whenever \mathbf{d} and \mathbf{p} are null, the cone is quadratic, \mathcal{Q}^{n+1} . The two are related by the following change of variables and notation:

$$\begin{cases} t = \mathbf{p}_i^T \mathbf{x} + q_i \\ \mathbf{s} = F_i \mathbf{x} + \mathbf{d}_i \end{cases} \Leftrightarrow (t, \mathbf{s}) \in \mathcal{Q}^{m+1} \quad (7)$$

where $F_i \mathbf{x} \in \mathbb{R}^m$. Though at first look Problem 6 does not look too different from Problem 5, it still needs to go through some classical techniques, called *equivalent transformation*, *relaxation*, and *successive linearization*.

Equivalent transformation This transformation is called exact convexification [15, 20] or lossless convexification [21] technique since the solution of the transformed problem is also the solution of the original problem. It is widely used to convexify objective functions that cannot be discretized as linear functions. Indeed, despite Eq. (5a) being the discretization of Eq. (2), they both still include the norm of the control vector in the optimization function, which is nonlinear. By adding a slack variable, a nonlinear optimization function can be turned into a linear optimization function and a quadratic constraint:

$$\begin{aligned} \text{Eq. (5a)} \quad \equiv \quad & \min \quad \sum_i u_i \cdot \Delta t \\ & \text{s.t.} \quad \|\mathbf{u}_i\| = u_i \end{aligned} \quad (8)$$

Once the control is discretized and transformed, it is possible to decide whether to solve the optimization in acceleration, thus keeping u_i as the optimization variable, or to add maneuvers as $\Delta \mathbf{v}_i$ at each node, hence solving the optimization in velocity. These two approaches bring different advantages: the former allows for an accurate representation of LT maneuvers but cannot describe impulses, while the latter allows for an easy description of both types of propulsion, with the assumption that the maximum allowed impulse at each node is equivalent to the resulting variation with constant LT acceleration over two consecutive nodes: $\Delta v_{i,i+1} = a_{S/C} \Delta t$. Due to the ease of description of both types of propulsion, the velocity formulation was chosen for this work. At each node, a possible maneuver is thus hypothesized, which is bounded by Δv_{MAX} , which is the maximum available maneuver at each node.

Relaxation Equation (8) linearized the optimization function introducing a quadratic constraint. This is, however, non-convex but can be turned into a second-order cone constraint by relaxing the equality:

$$\|\mathbf{u}_i\| = u_i \xrightarrow{\text{Relax.}} \|\mathbf{u}_i\| \leq u_i \Leftrightarrow (u_i, \mathbf{u}_i) \in \mathcal{Q}^4, \quad \forall i \in \mathbb{N}_{[0,N]}. \quad (9)$$

Equation (1d) on the other hand is already relaxed and the following holds:

$$\left(2M, \sqrt{\Sigma_{t_j}} (\mathbf{x}_i - \boldsymbol{\mu}_{t_j}) \right) \in \mathcal{Q}^7, \quad j = \{0, f\}, i = \{0, N\}. \quad (10)$$

Though the relaxation is introducing a larger feasible set than the original problem, Eq. (9) will always reach equality at the optimal point, since the goal is to minimize $\|\mathbf{u}\|$, meaning the relaxation is also a lossless convexification technique.

Successive linearization The previous techniques introduced slack variables and relaxed constraints without modifying the solution of the original problem. Successive linearization, instead, does introduce a simplification, in that the original nonlinear problem is substituted with a first-order Taylor expansion around the initial ballistic trajectory, referred to as $\tilde{\mathbf{x}}$. Remembering that at each node there are 9 optimization variables from Section 2.2 - plus 1 slack variable through the equivalent transformation - it is possible to discretize the influence of maneuvers and deviations from the ballistic trajectory with:

$$\mathbf{x}_{i+1} \approx \tilde{\mathbf{x}}_{i+1} + [R_i | M_i] \begin{bmatrix} \mathbf{x}_i - \tilde{\mathbf{x}}_i \\ \Delta \mathbf{v}_i - \Delta \tilde{\mathbf{v}}_i \end{bmatrix}, \quad (11)$$

where $i \in \mathbb{N}_{[0,N]}$, the initial reference velocity variation $\Delta \tilde{\mathbf{v}}_i$ is null, and $R_i \in \mathbb{R}^{6 \times 6}$, $M_i \in \mathbb{R}^{6 \times 3}$ are the state transition matrices (STMs), which respectively map deviations in the states and velocity to the next node. Due to linearization, iterations k may be necessary to accurately solve the original problem: the optimization can thus be repeated following a standard successive convex optimization approach, where the new trajectory is convexified, until the solution of the optimization and the accurate forward propagation of the maneuvering orbit match to a prescribed accuracy, that is until two consecutive successive iterations yield the same optimization vector. However, successive convexification does not hold the same mathematical properties as a single convexification. Hence, it is also important to identify the state coordinates for which linearization holds for larger variations, such that the iterative process is not triggered.

3 Handling uncertain constraints

The optimization finds a deterministic path for this OCP. However, the boundary constraints are uncertain, since the initial and final deviations to be found are not purely geometrical but hold a statistical meaning: the further from the mean states the final solution is, the less probable the path found is to happen. By simply constraining the initial and final deviations to be less than a value as in Eq. (1d), the optimizer will see the deviations as “free propellant” hence taking full advantage of them, but actually creating the least probable path, among the possible ones. At the optimum, the relaxed bound will, indeed, be exact.

Two different approaches can then be followed, depending on the information sought. If an indication on whether the maneuver has happened or not is wanted, it is possible to set a bound on the maximum allowed Mahalanobis distance. The optimization will then return the minimum Δv required to link the states with the chosen confidence. With just a few runs with different bounds it is then possible to obtain an indication on the probability that a maneuver has happened. This is sketched in Fig. 1a. However, the optimization always finds the optimum on the ellipsoid, hence hindering the a-posteriori statistical analysis. For this reason, if an accurate statistics of the maneuver is sought, the initial and final states variations cannot be determined within the optimization but need to be defined beforehand, shown in Fig. 1b. The fourth-order CUT [22] was chosen to do so: by running the optimization $N^2 + 2N + 1$ times, where $N = 12$ is the dimension of the problem, it is possible to reconstruct a-posteriori the first four moments - mean, variance, skewness, and kurtosis - of the final maneuver profile distribution, thus allowing for the analysis of the effect of uncertainty in the states on the overall maneuver existence and estimation. Sigma points drawn from the initial and final covariance determine the initial and final deviations, so that the cone constraint in Eq. (10) is substituted by:

$$\begin{bmatrix} \mathbf{x}_0 - \boldsymbol{\mu}_{t_0} \\ \mathbf{x}_N - \boldsymbol{\mu}_{t_f} \end{bmatrix}_c = \Delta \mathbf{X}_{CUT4,c}^{12 \times 1} \quad c \in \mathbb{N}_{[1, N^2 + 2N + 1]} \quad (12)$$

where for each c the optimization is run. The superiority in efficiency of the CUT with respect to a simple Monte Carlo (MC) run and other cubature methods is detailed in [23]. Note that also with this construction the ballistic trajectory is only computed once and holds for all CUT iterations, since deviations are linearly propagated through STMs.

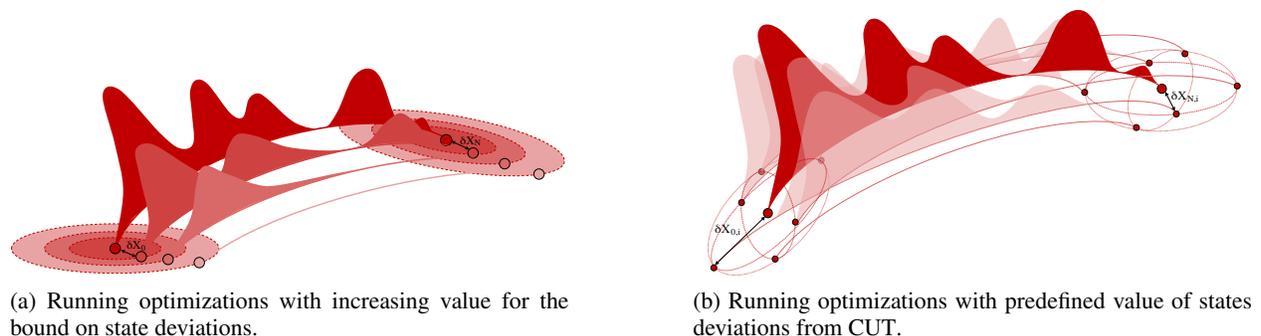


Figure 1: Dealing with uncertain constraints inside (left) and outside (right) the optimization routine, by respectively successively constraining the Mahalanobis distance value and using the CUT-4 algorithm.

4 Finalization of the SOCP problem

Now that the original problem is turned into a SOCP and the uncertain nature of the bounds is taken care of, it is possible to enunciate the formulation to be solved. In order to make the description clearer, refer to Fig. 2 for the remainder of the Section. Suppose two states - the outcome of an OD [24] - are available at two epochs, simplified with a black dot and a shaded ellipse, $(\boldsymbol{\mu}_{t_0}, \Sigma_{t_0})$, $(\boldsymbol{\mu}_{t_f}, \Sigma_{t_f})$. The state at the earliest epoch is propagated forward to the second one, determining a reference trajectory, white solid line. The propagated and determined states will not correlate with typical data association techniques [1, 25, 26], but correlation may be recovered assuming a maneuver has happened. The time interval is then discretized in $N+1$ nodes, black squares on white line, and an impulsive maneuver Δv_i is hypothesized at every node. From Eq. (11), STMs M_i and R_i are used to map the maneuvers’ and state deviation effects forward in time. The cumulative effect of all maneuvers and initial deviation allows the state at \mathbf{x}_N to reach the desired location. The complete successive convex optimization problem with the CUT-4 approach is summarized in Table 1. This problem can be solved by primal-dual interior-point methods. We use MOSEK through

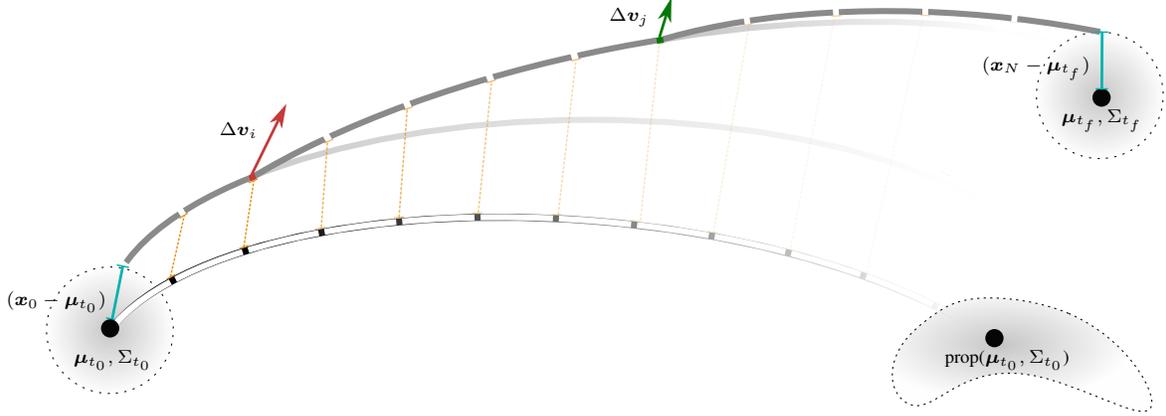


Figure 2: Initial sampled trajectory (white line with black squares), initial deviation (blue) and mid-course maneuvers (red and green) to match final deviation (blue).

its MATLAB interface⁴, while Differential Algebra (DA)⁵ is used to automatically compute the STMs. Though no bounds on optimization variables are needed for the problem to converge, they are included to obtain realistic solutions. The Δv s are bounded for physical purposes, as stated before, so that the achievable maneuver can be obtained by the on-board propellant:

$$0 \leq \Delta v_i \leq \Delta v_{MAX}, |\Delta v_{il}| \leq \Delta v_{MAX} \quad \forall i \in \mathbb{N}_{[0,N]}, \forall l = x, y, z, \quad (13)$$

States, on the other hand, are bounded due to the linearization: a large state variation may introduce a significant error on the linearized dynamics, hence needing more iterations to converge:

$$\Delta x_{ij,MIN} \leq x_{ij} - \tilde{x}_{ij} \leq \Delta x_{ij,MAX}, \quad \forall i \in \mathbb{N}_{[0,N]}, \forall j \in \mathbb{N}_{[1,6]} \quad (14)$$

It is expected that highly varying coordinates such as cartesian coordinates (CC) take longer to converge to a solution than, for example, modified equinoctial elements (MEE). Indeed, examples in Section 5 will show that MEE are the preferred choice due to having only one fast variable and no singularities.

Table 1: Pseudo-code of the successive convex optimization algorithm for maneuver detection and estimation. The *for*-loop is not performed when the Mahalanobis distance approach is taken.

Initial guess	$x_i^0 = \tilde{X}_i^0, \quad \Delta v_i^0 = \Delta \tilde{v}_i^0 = \mathbf{0} \quad \forall i \in \mathbb{N}_{[0,N]}$	<i>Ballistic trajectory</i>
for $c \in \mathbb{N}_{[1, N^2+2N+1]}$		<i>Loop on CUT-4 sigma points</i>
do		
min	$\sum_{i=0}^N \Delta v_i^k,$	
s.t.	Eq. (11)	<i>Continuity of trajectory</i>
	Eq. (5d) [No <i>for</i> -loop], or Eq. (12)	<i>Initial and final states variation</i>
	Eq. (9)	<i>Cone constraint on Δv norm</i>
	Eq. (13)	<i>Bound on Δv</i>
	Eq. (14)	<i>Bound on state variation</i>
	while ($\ sol^k - sol^{k-1}\ > \epsilon$)	<i>Successive convexification</i>
end		

5 Maneuver detection and estimation results

This section shows some test cases in which the exact reconstruction, the detection and lastly the estimation of maneuvers are performed. Firstly, the estimation of a synthetic maneuver is carried out, to show the LT and impulsive

⁴<https://docs.mosek.com/9.0/toolbox/index.html>

⁵<https://github.com/dacelib/dace>

reconstructions for perfect states. Then the Mahalanobis distance approach is shown for two cases taken from EUMETSAT publicly available dataset for an EWSK maneuver and a non-maneuvering object. This will highlight the maneuver detection feature. Lastly, the CUT approach is used for the same EWSK maneuver and for the LT orbit raise from geostationary transfer orbit (GTO) to GEO, to showcase the maneuver estimation feature. The very large deviation from the reference trajectory will highlight the different behaviors of the coordinate systems. These very different orbits and maneuver types will showcase the versatility and tailorability of the approach.

5.1 Synthetic maneuver estimation

Maneuvers were initially simulated to test the algorithm, given known dynamics and perfect states. This was to test the accurate reconstruction of the maneuvers. Figure 3 shows the reconstruction of a 1 m/s out-of-plane maneuver performed 5 h after the availability of the first state in keplerian dynamics. As shown in Section 2, the initial trajectory dynamics is a plug-in, meaning any type of dynamics can be accommodated. In this case, keplerian dynamics was used to estimate the maneuver, so that it matched the dynamics of the object. The initial GEO trajectory was sampled every minute. Two reconstructions were performed to show the effect of the maximum allowed Δv at each node on the final profile: the unconstrained reconstruction (green) matches the impulsive input data, while the LT reconstruction symmetrically spans around the maneuver epoch with a $\Delta v_{MAX} = 6$ mm/s. To obtain the desired maneuver, then, 167 small impulses were needed, summing up to 2.8 h, which is the exact span estimated.

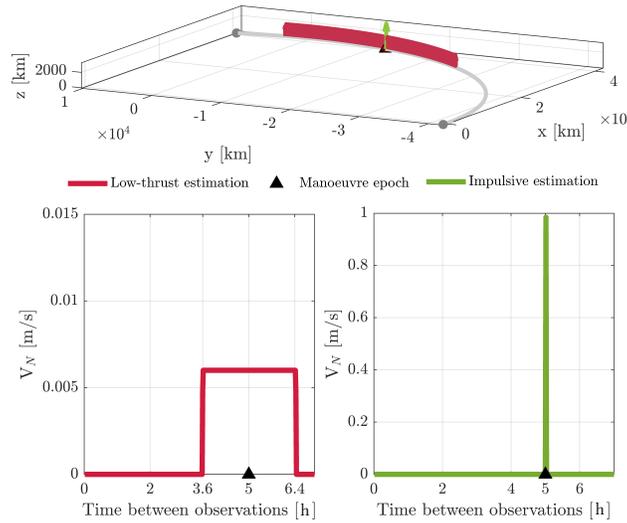
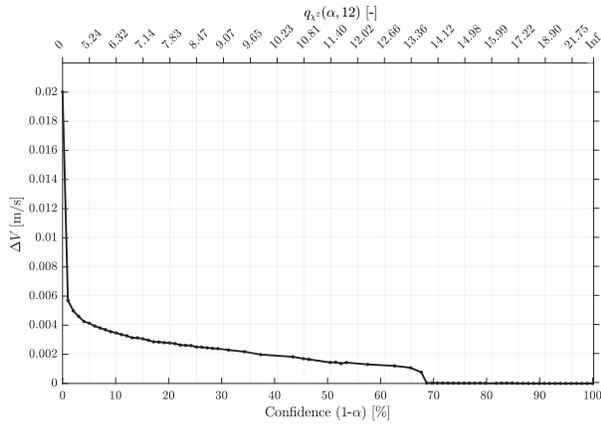


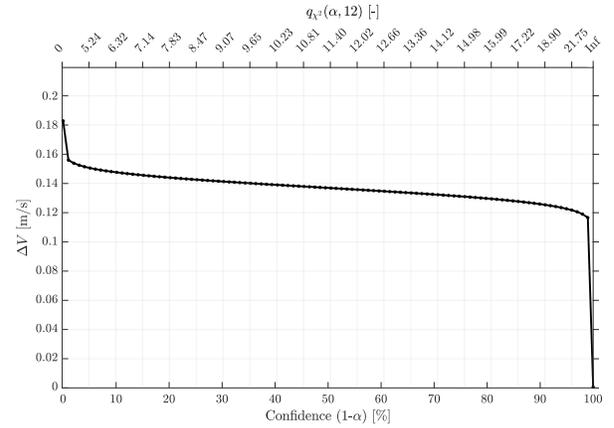
Figure 3: Manoeuvre profile estimation of a simulated manoeuvre with LT (left) and impulsive (right) assumption.

5.2 Mahalanobis distance approach

With the Mahalanobis distance approach, the states uncertainties are bounded by the ellipsoid defined in Eq. (4), where the value of \mathcal{M} depends on the confidence level α . The resulting maneuver profile represents the smallest maneuver achievable with the given confidence on the states. The larger the confidence, the larger is the search space around the mean state, hence the smaller the connecting maneuver can be. At the extreme, with $\alpha = 0$ - hence 100% confidence - the associated χ^2 quantile is infinite, hence always finding a ballistic solution to connect the two orbits. Figure 4 shows the total maneuver magnitude depending on the confidence chosen for two different cases taken from EUMETSAT public dataset, one where an EWSK maneuver is performed, and one where no maneuver is performed. Usually confidences of 95% or more are used in statistics to perform these kinds of analyses, hence showing that for Fig. 4a there exists a ballistic solution which can connect the two orbits, while for Fig. 4b a residual maneuver of at least $\Delta V = 0.12$ m/s is needed to connect the two orbits with the same confidence. For comparison purposes, the accumulated Δv over a week for the SRP perturbation is $\Delta V_{SRP} = 0.007$ m/s. This is a very efficient way to detect maneuvers, as the STM creation for 50 nodes takes 0.7 s and the optimisation takes 25 ms for the case at hand.



(a) Maneuver detection run on two states a week apart with no maneuver involved. There exists a ballistic solution starting from 68% confidence.



(b) Maneuver detection run on two states a week apart with an EWSK maneuver involved. A ballistic solution is never .

Figure 4: Evolution of minimum Δv required to connect two states depending on confidence level chosen.

5.3 CUT approach

Differently from the Mahalanobis distance approach, the CUT approach can not only detect, but also estimate the maneuver profile and its higher order moments by running the optimization $N^2 + 2N + 1$ times. This means that the maneuver estimation comes at the expense of more computational power needed. Section 5.3.1 shows the estimation of the same EWSK maneuver analysed in Section 5.2, applying a further filter to the maneuver estimation process, that is the possibility to shrink the search window within a specific revolution. Section 5.3.2 instead estimates a very large LT maneuver, hence introducing a large deviation from the reference trajectory. In this scenario, the choice of coordinates will greatly impact the computation of the maneuver.

5.3.1 EWSK maneuver in GEO: reducing the maneuver window

EUMETSAT releases weekly updates of their METEOSAT satellites' states and covariances, including maneuvers types and times, if available. By estimating the maneuver, one can thus check whether the available data matches the reconstructed ones. However, having data for GEO satellites available every seven days, the same routine maneuver opportunity presents itself at each period, meaning a simple impulse may be split over seven different occasions, as shown in Fig. 5, where the very low-thrust (VLT) reconstruction greatly highlights this pattern. To exploit this information about the maneuver and simultaneously reduce the computational effort, the nodes were not evenly placed on the entire seven days window, but only defined on a portion of it. To do so, an estimate of the maneuver epoch was found by looking for the minimum distance between the forward propagation of μ_{t_0} and the backward propagation of μ_{t_f} , then a symmetric interval was chosen around that epoch. The dashed column of Fig. 5 shows the new restricted window with the impulsive (red) and constrained (green) maneuver reconstruction.

For the constrained reconstruction, $\Delta v_{MAX} = 0.021$ m/s was chosen for each node, due to lack of accurate data for the satellite. It can be noted that the estimated peak matches with the real maneuver epoch. While Fig. 5 was reconstructed with the assumption of perfect states, Fig. 6 shows the complete reconstruction with a restricted window after the application of the CUT-4 algorithm. The green profile matches Fig. 5 solution being the first sigma point considered in the CUT-4. The total estimated maneuver was $\Delta V = 0.18896$ m/s, which fits in the typical range for EWSK maneuvers, which sits between 0.05 and 0.2 m/s [27]. The bottom right plot in Figure 6 shows the probability distribution, boxplot, and violin plot of the reconstructed maneuver magnitude. This was performed by fitting a Pearson distribution in the four moments estimated through the CUT-4. As can be seen, estimating the skewness $s = 0.7$ and kurtosis $k = 2.52$ parameters is fundamental to reconstruct the non-gaussian profile. This is especially evident for very small maneuvers where the left tail of the distribution is much smaller than the right tail. The cumulative distribution function of the estimated maneuver can then be used if competing reconstructions are estimated to find the most probable, as done in [10]. The initial trajectory with STMs creation took 0.7 s (same process as for the Mahalanobis distance approach), each optimization took 5 – 30 ms, for a total of 22 s with parallelization in Matlab. The CUT approach thus takes advantage of the STM creation and uses the output for all optimizations to cut the overall computational time.

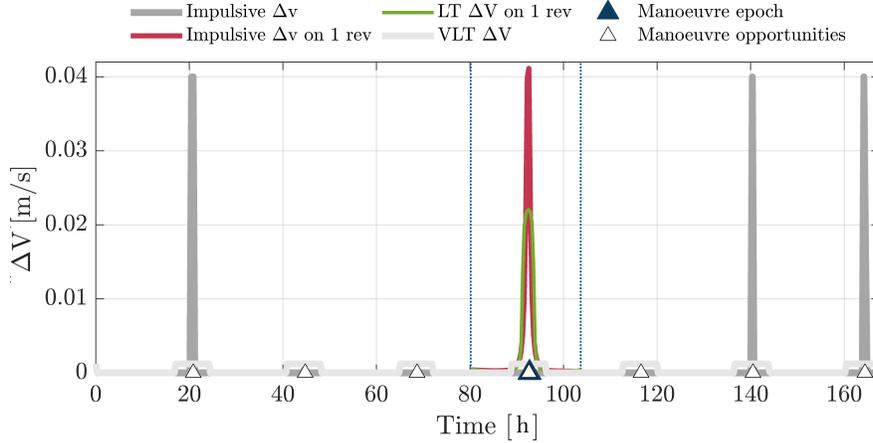


Figure 5: EWSK maneuver estimation on a seven days window and on a restricted one day window with impulsive and LT assumption. Seven maneuver occasions are found, among which the real manoeuvre epoch. Estimation is performed on the assumption of perfect states.

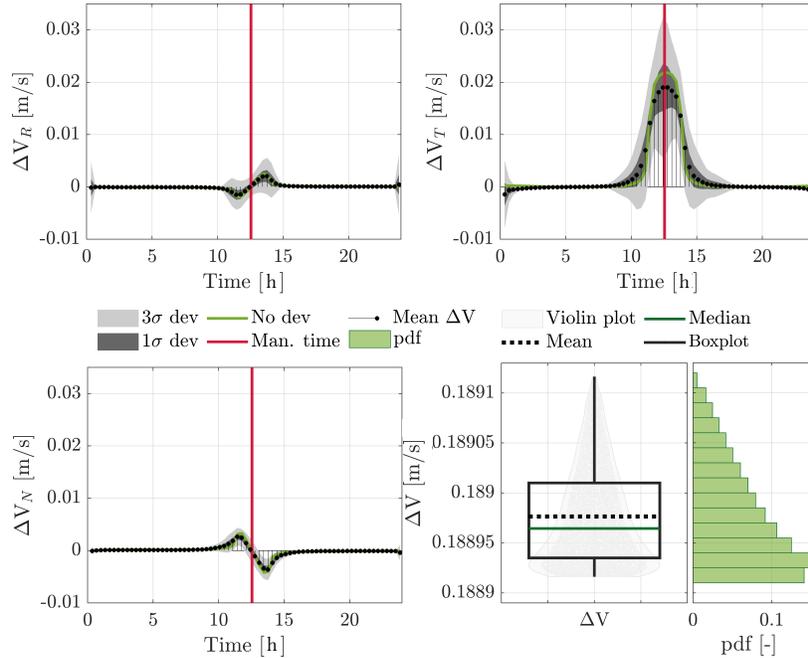


Figure 6: EWSK maneuver estimation for radial (R), tangential (T), and normal (N) components on a restricted one period window, with a-posteriori probability density reconstruction through the use of the CUT-4 algorithm.

5.3.2 LT orbit raise maneuver from GTO to GEO: choosing the right coordinates

For this test case we obtained tracking data of MEV-2 from Defence Agency Technology (DTA). States and covariances were then obtained through our in-house initial orbit determination (IOD) algorithm [1], the solution of which was then fed to our Differential Algebra Least Squares (DALs) algorithm [24]. Low-thrust maneuvers were then estimated with a maximum acceleration of $a = 0.22 \text{ mm/s}^2$. This case, differently from the EWSK maneuver, involved a large maneuver on a highly elliptical orbit. It was thus of interest to understand the convergence of the algorithm depending on the coordinates used. For this reason, the maneuver was firstly reconstructed on the assumption of a perfect state for CC, classical orbital elements (COE) and MEE. Results are shown in Fig. 7. It can be seen that all coordinates reached convergence on the same maneuver pattern. However, COE and MEE did not need any successive

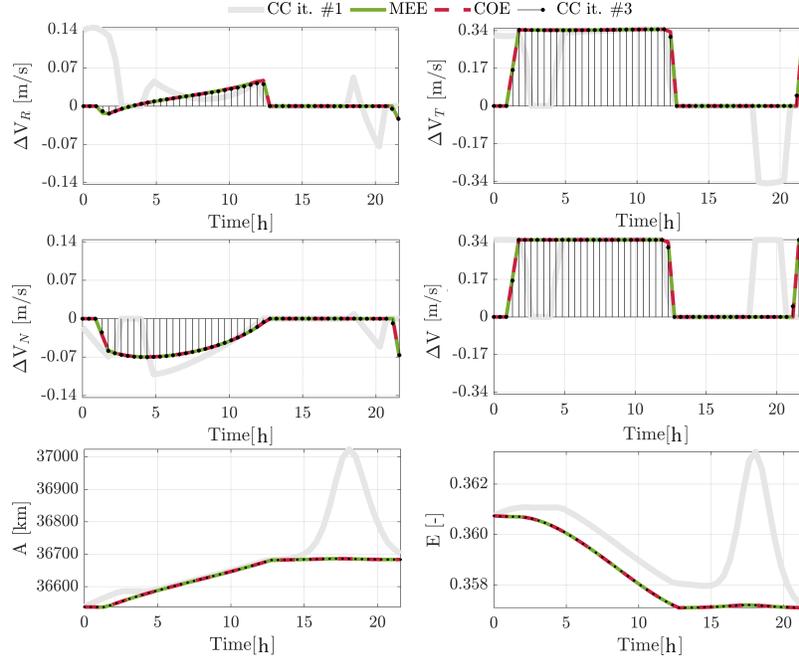


Figure 7: LT maneuver reconstruction with different coordinates. CC need three successive convexifications to reach convergence, while COE and MEE do not need any iterations. Non-convergence on first iteration is visible in the semimajor axis and eccentricity evolution (bottom).

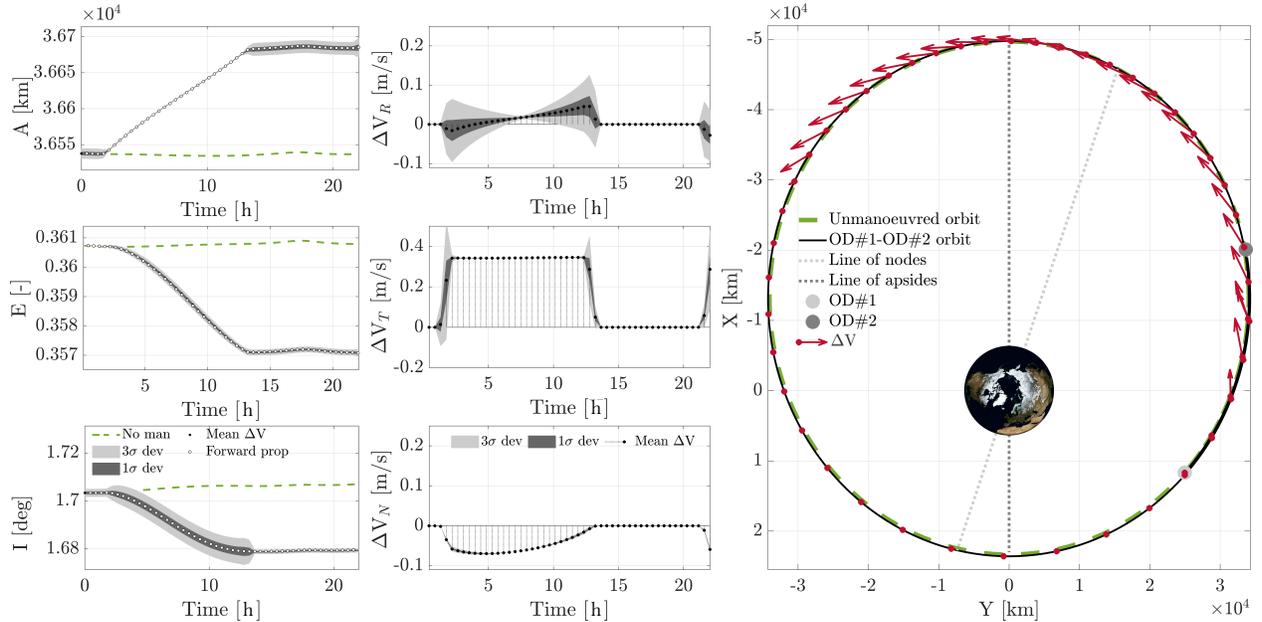


Figure 8: LT maneuver estimation for an orbit raise by MEV-2 from GTO to GEO. The orbital elements variation (left) and maneuver profile in RTN components (middle) are reconstructed showing mean and 3σ deviation through the CUT-4 algorithm. The maneuvers location along the orbit is shown on the right. Forward propagation of the obtained maneuver profile is also shown in the left plot.

convexification, while CC needed three iterations to reach convergence. The reconstructed patterns on the semimajor axis and eccentricity highlight the initial difficulty, where the linearization was not accurate. This was expected, due to the fast varying nature of all components of CC, as anticipated in Section 2.3. Despite all coordinates types reaching

the same maneuver pattern, CC performed the worst in terms of computation time, needing three successive convex optimizations to reach the same conclusion. Figure 8 shows the complete reconstruction with elements evolution, maneuver profile, and orbital positioning of the maneuver obtained with MEE. Given that a change in the orbit shape and inclination happened, maneuvers were estimated around the line of apsides and the line of nodes, respectively, as expected. In the left plot, the validation is also shown: the white dots are the forward propagation implemented with the maneuver pattern estimated in the middle plot showing that the solution of the convexified problem also solved the original problem. The total maneuver was estimated to be $\Delta V = 9.1$ m/s and took 8.5 min: 2.6 s for the trajectory and STMs generation with 50 nodes, around 0.37 – 0.83 s for each optimization, parallelized in Matlab for 4121 samples. The computational burden is thus due to the wish to estimate the ΔV statistical properties.

Figure 9 shows the reconstructed Pearson distribution’s probability density, boxplot, and violin plot. This time $s = 0.019$ and $k = 2.994$ meaning the distribution can be, in first approximation, considered gaussian. The choice of using the CUT-4 algorithm thus allowed us to estimate different output statistics.

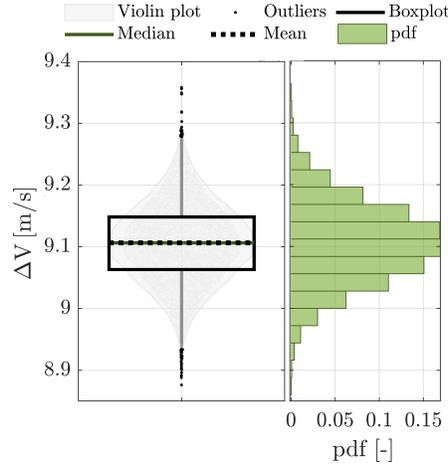


Figure 9: A-posteriori probability density reconstruction by fitting a Pearson distribution in the first four moments. The maneuver magnitude can in first approximation be considered Gaussian.

6 Conclusions

This article introduced a novel method to detect and estimate a maneuver between two orbits exploiting convex optimization, with the only assumption that maneuvers were performed optimally. The minimum-fuel OCP was transformed from a NLP problem to a SOCP problem to exploit the benefits of convex optimization: polynomial run-time complexity and convergence to the global optimum. The problem was discretized in time, STMs were generated to linearly propagate the influence of maneuvers on the initial accurate trajectory, and a limit on the impulsive ΔV was set to accommodate for different propulsion systems. In the end, it was possible to use successive convex optimization problems in case the optimum solution of the SOCP was not the solution of the NLP problem due to linearization. Results were shown for an out-of-plane maneuver in keplerian dynamics, an EWSK maneuver in GEO and a LT orbit raise from GTO to GEO, to highlight the versatility of the approach. CC was fine to reconstruct the first two cases, but needed successive iterations to converge for the latter test, while COE and MEE did not need any iteration, with the forward propagation of the maneuvering orbit always matching the SOCP solution. Uncertainty in the initial and final states was dealt with through the Mahalanobis distance and CUT-4 approaches, which allowed for the detection of the maneuver and then estimation of mean, variance, skewness, and kurtosis parameters. By fitting a Pearson statistics through the four moments it was possible to show that the ΔV statistics did not necessarily follow a Normal distribution. The tailorability of the approach was also shown by automatically restricting the search time window and using different dynamics.

Acknowledgements

The work presented is supported by AOARD under Grant FA2386-21-1-4115. The authors are grateful to Dr Jovan Skuljan of DTA for providing data and constructive discussions.

References

- [1] Laura Pirovano, Daniele A. Santeramo, Roberto Armellin, Pierluigi Di Lizia, and Alex Wittig. Probabilistic data association: the orbit set. *Celestial Mechanics and Dynamical Astronomy*, 132(2):15, 2020.
- [2] Xuefeng Tao, Zhi Li, Qiuwu Gong, Yasheng Zhang, and Ping Jiang. Uncertainty analysis of the short-arc initial orbit determination. *IEEE Access*, 8:38045–38059, 2020.
- [3] M. Losacco, R. Armellin, C. Yanez, S. Lizy-Destrez, L. Pirovano, and F. Sanfedino. Robust initial orbit determination for short-arc doppler radar observations. *arXiv preprint arXiv:2204.13966*, 2022.
- [4] Laura Pirovano, Roberto Armellin, Jan Siminski, and Tim Flohrer. Differential algebra enabled multi-target tracking for too-short arcs. *Acta Astronautica*, 182:310–324, 2021.
- [5] Laura Pirovano, Gennaro Principe, and Roberto Armellin. Data association and uncertainty pruning for tracks determined on short arcs. *Celestial Mechanics and Dynamical Astronomy*, 132(1):6, January 2020.
- [6] Russell P. Patera. Space event detection method. *Journal of Spacecraft and Rockets*, 45(3):554–559, 2008.
- [7] Stijn Lemmens and Holger Krag. Two-line-elements-based maneuver detection methods for satellites in low earth orbit. *Journal of Guidance, Control, and Dynamics*, 37(3):860–868, 2014.
- [8] Byron D. Tapley, Bob E. Schutz, and George H. Born. Chapter 4 - fundamentals of orbit determination. In Byron D. Tapley, Bob E. Schutz, and George H. Born, editors, *Statistical Orbit Determination*, pages 159–284. Academic Press, Burlington, 2004.
- [9] Daniel P Lubey. *Maneuver Detection and Reconstruction in Data Sparse Systems with an Optimal Control Based Estimator*. dissertation, University of Colorado Boulder, 2015.
- [10] Marcus J. Holzinger, Daniel J. Scheeres, and Kyle T. Alfriend. Object correlation, maneuver detection, and characterization using control-distance metrics. *Journal of Guidance, Control, and Dynamics*, 35(4):1312–1325, 2012.
- [11] Navraj Singh, Joshua T. Horwood, and Aubrey B. Poore. Space object maneuver detection via a joint optimal control and multiple hypothesis tracking approach. *Advances in the Astronautical Sciences*, 143(January):843–862, 2012.
- [12] Alessandro Morselli, Roberto Armellin, Pierluigi Di Lizia, and Franco Bernelli Zazzera. A high order method for orbital conjunctions analysis: Sensitivity to initial uncertainties. *Advances in Space Research*, 53(3):490–508, 2014.
- [13] Charles H. Acton. Ancillary data services of nasa’s navigation and ancillary information facility. *Planetary and Space Science*, 44(1):65 – 70, 1996.
- [14] Danylo Malyuta, Taylor P Reynolds, Michael Szmuk, Thomas Lew, Riccardo Bonalli, Marco Pavone, and Behçet Açı kmeşe. Convex optimization for trajectory generation. *arXiv preprint arXiv:2106.09125*, 2021.
- [15] Xinfu Liu, Ping Lu, and Binfeng Pan. Survey of convex optimization for aerospace applications. *Astrodynamics*, 1(1):23–40, 2017.
- [16] Andrea Carlo Morelli, Christian Hofmann, and Francesco Topputo. Robust low-thrust trajectory optimization using convex programming and a homotopic approach. *IEEE Transactions on Aerospace and Electronic Systems*, 58(3):2103–2116, 2022.
- [17] Xuewen Liu, Hongwei Yang, and Shuang Li. Collision-free trajectory design for long-distance hopping transfer on asteroid surface using convex optimization. *IEEE Transactions on Aerospace and Electronic Systems*, 57(5):3071–3083, 2021.
- [18] Behçet Açı kmeşe, John M. Carson, and Lars Blackmore. Lossless convexification of nonconvex control bound and pointing constraints of the soft landing optimal control problem. *IEEE Transactions on Control Systems Technology*, 21(6):2104–2113, 2013.
- [19] Roberto Armellin. Collision avoidance maneuver optimization with a multiple-impulse convex formulation. *Acta Astronautica*, 186:347–362, 2021.
- [20] Steven H. Low. Convex relaxation of optimal power flow—part ii: Exactness. *IEEE Transactions on Control of Network Systems*, 1(2):177–189, 2014.
- [21] Behçet Açı kmeşe and Lars Blackmore. Lossless convexification of a class of optimal control problems with non-convex control constraints. *Automatica*, 47(2):341–347, 2011.

- [22] Nagavenkat Adurthi, Puneet Singla, and Tarunraj Singh. The conjugate unscented transform — an approach to evaluate multi-dimensional expectation integrals. In *2012 American Control Conference (ACC)*, pages 5556–5561, 2012.
- [23] Nagavenkat Adurthi, Puneet Singla, and Tarunraj Singh. Conjugate Unscented Transformation: Applications to Estimation and Control. *Journal of Dynamic Systems, Measurement and Control, Transactions of the ASME*, 140(3):1–22, 2018.
- [24] Matteo Losacco, Gennaro Principe, Roberto Armellin, Laura Pirovano, David Gondelach, Juan Felix San Juan, Martin Lara, Raul Dominguez Gonzalez, Fernando Pina Caballero, and Igone Urdampilleta. Differential Algebra-based Orbit Determination with the Semi-analytical Propagator SADA. *8th European Conference on Space Debris*, april 2021.
- [25] Keric Hill, Kyle Alfriend, and Chris Sabol. Covariance-based uncorrelated track association. In *AIAA/AAS Astrodynamics Specialist Conference and Exhibit*, page 7211, 2008.
- [26] Jan A. Siminski, Oliver Montenbruck, Hauke Fiedler, and Thomas Schildknecht. Short-arc tracklet association for geostationary objects. *Advances in Space Research*, 53:1184–1194, April 2014.
- [27] W.J. Larson and J.R. Wertz. *Space Mission Analysis and Design*. Space technology library. Microcosm, 1992.